Fizika Nizkikh Temperatur, 1997, v. 23, No 9, p. 951–964

Point-contact-spectroscopy evidence of quasi-particle interactions in RNi_2B_2C (R = Ho, Y)

I. K. Yanson[1,2], V. V. Fisun[1,2], A. G. M. Jansen[1], P. Wyder[1], P. C. Canfield[3], B. K. Cho[3], C. V. Tomy[4], and D. McK. Paul[4]

[1]*Grenoble High Magnetic Field Laboratory, Max-Planck-Institut für Festkörperforschung and Centre National de la Recherche Scientifique, B.P. 166, F-38042 Grenoble Cedex 9, France*

[2]*B. Verkin Institute for Low Temperature Physics and Engineering, National Academy of Sciences of Ukraine, 310164 Kharkov, Ukraine*
E-mail: fisun@ilt.kharkov.ua

[3]*Ames Laboratory, Iowa State University, Ames, IA 50011, USA*

[4]*Department of Physics, University of Warwick, Coventry CV4 7AL, UK*

Submitted March 24, 1997

The point-contact (PC) d^2V/dI^2-spectra of $HoNi_2B_2C$ and YNi_2B_2C reveal structure at applied voltages corresponding to the phonon frequencies. At about 4 meV a maximum is observed in the phonon density of states by analogy to the soft-phonon structure in neutron scattering experiments for $LuNi_2B_2C$ [P. Dervenagas et al., *Phys. Rev.* **B52**, R9839 (1995)] and YNi_2B_2C [H. Kawano et al., *Czech. J. Phys.* **46**, S2–825 (1996), *Phys. Rev. Lett.* **77**, 4628 (1996)]. In the Ho compound the low-energy phonon peak is suppressed by an applied magnetic field in an anisotropic way, pointing to an interaction between the phonons and the magnetic systems. Surprisingly, in the nonmagnetic Y compound the 4-meV peak is also suppressed by a magnetic field. In the Ho-compound contacts which show the «quasi-thermal» behavior, the detailed magnetic-field and temperature dependences of the PC spectra suggest that the magnetic order is destroyed due to the coupled phonon-magnon subsystem which is driven out of equilibrium by electrons that pass through the contact, by analogy with the nonequilibrium phonon-induced destruction of the superconducting state in point contacts [I. K. Yanson et al., *JETP Lett.* **45**, 543 (1987)]. The PC electron-phonon interaction (EPI) spectral functions are reconstructed and the estimates for the λ-parameter yield values of the order of 0.1. Comparison with PC EPI spectra of nonsuperconducting and nonmagnetic $LaNi_2B_2C$ [I. K. Yanson et al., *Phys. Rev. Lett.* **78**, 935 (1997)], as well as the comparative study of PC EPI and Andreev-reflection spectra for various contacts with superconducting Ho and Y compounds suggest that the low-energy part of the electron-quasi-particle interaction spectral function is responsible for the Cooper pairing in these materials.

PACS: 74.70.Ad, 74.25.Kc, 73.40.Jn, 72.10.Di

1. Introduction

The recently discovered intermetallic compounds [1,2] (RNi_2B_2C (R = rare earth, Y, Sc, Th) show a very rich interplay between superconductivity and magnetism with higher superconducting and magnetic critical temperatures compared with the rare-earth rhodium borides and molysulfides (selenides) magnetic superconductors [3]. These materials are now being studied intensively by various experimental techniques [4–10]. However, there are only a few reports concerning the application of the tunneling spectroscopy method [11–14]. All of them deal with the nonmagnetic compounds. This circumstance is probably attributable to the difficulties in preserving the fine balance between intra- and inter-layer magnetic interactions at the tunnel junction interfaces with the magnetic compounds.

The point-contact spectroscopy (PCS) involves studies of the nonlinearities of current-voltage characteristics of metallic constrictions with characteristic size d smaller than the inelastic electron mean free path l_{in} [15,16]. In contrast with a tunneling junction, an ideal point contact has no interfaces. In the case of a junction made of dissimilar electrodes, PCS has the advantage that the material is probed into the depth of the current

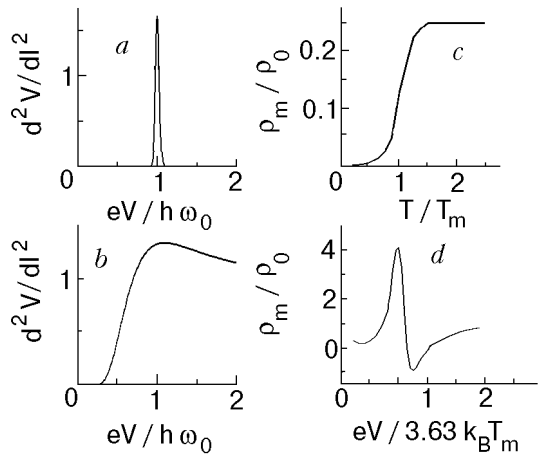

Fig. 1. Schematic diagrams of the PC d^2V/dI^2-spectra for an Einstein-type phonon spectrum for the spectroscopic (either ballistic or diffusive) (*a*) and thermal (*b*) regimes of current flow. Theoretical $d^2V/dI^2(V)$ dependence (*d*) calculated in the thermal limit for the $\rho_m(T)$ dependence [17] (*c*); ρ_0 is the residual resistivity of a metal.

spreading region, which is of the order of the constriction size. On one side, this size may be large enough to make a negligible contribution of the spoiled interface layers to the point-contact spectrum; on the other side it may be not too large with respect to the condition of the spectroscopic regime of current flow,

$$d \le \min\,(l_{\text{in}}\,,\ \sqrt{l_{\text{in}} l_e}\ ), \qquad (1)$$

where l_e is the elastic scattering mean free path.

The voltage dependence of the differential resistance of a ballistic point contact reflects the energy-dependence of the scattering cross section of the conduction electrons, such that the point-contact spectra [$d^2V/dI^2(V)$ dependences] are proportional to the electron-phonon-interaction (EPI) spectral function. In the case of point contacts between different metals with strongly different Fermi velocities, only the spectrum of the material with the smaller Fermi velocity v_F is seen [16]:

$$\frac{d \ln R}{dV}(V) = \frac{4}{3}\frac{ed}{\hbar v_F} g_{PC}(\omega)\Big|_{\hbar\omega = eV}\ ; \quad (T \simeq 0)\ . \qquad (2)$$

The function $g_{PC}(\omega) = \alpha^2_{PC}(\omega)F(\omega)$ is similar to the Eliashberg function. Here $\alpha^2_{PC}(\omega)$ is the averaged EPI matrix element with kinematic restrictions imposed by the contact geometry, and $F(\omega)$ is the phonon density of states. The contact diameter d is determined by the normal-state resistance at zero bias R_0 via the Sharvin expression [16]. In the case of copper $d \simeq 30/\sqrt{R_0[\Omega]}$ nm, which we shall use for further estimates.

In the spectroscopic regime [Eq.(1)] no heating of the contact area occurs. However, if the contact size is large compared with the electron energy-relaxation length $\Lambda_\varepsilon = \min\,(l_{\text{in}}\,,\ \sqrt{l_{\text{in}} l_e}\ )$, then there is a local heating of the contact with a maximum temperature T_0 at the center of the contact given by the Kohlrausch relation

$$V^2 = 4L(T_0^2 - T^2) \qquad (3)$$

for an applied voltage V across the contact at the bath temperature T. This relation transforms into $eV \simeq 3.63 k_B T_0$ or 1-mV applied voltage corresponds to 3.20-K temperature increase at the contact for the standard Lorentz number $L = 2.44\cdot10^{-8}$ V^2/K^2 (assuming $T = 0$). In the thermal regime the PCS-spectrum of an Einstein oscillator $\hbar\omega_0$ looks like a smeared step with a shallow maximum at $eV = 1.09\hbar\omega_0$ [17,18]. In Figs. 1,*a* and 1,*b* the point-contact spectra of the electron interaction with an Einstein phonon-mode are shown schematically for, respectively, the spectroscopic (either ballistic or diffusive) and the thermal regimes.

The thermal feature in the PC spectra can be quite sharp if a phase transition occurs at a particular temperature T_m, which leads to the jump-like increase of the temperature-dependent contribution $\rho_m(T)$ to the resistivity (see Fig. 1,*c*). Such a situation holds, for example, for the ferromagnetic metals (Ni, Fe) at the voltages corresponding to the Curie temperatures. In this case a maximum on the dV/dI curve and a sharp «N»-type feature on the second derivative d^2V/dI^2 (Fig. 1,*d*) appear at about $eV_m \simeq 3.63\ k_B T_m$ [17].

Similar peculiarities in the PC d^2V/dI^2 spectra of superconductors appear if the average concentration of quasi-particle excitations exceeds a critical value, destroying the superconducting order parameter in the contact region. It was found [19] that the voltage positions of these «*N*»-type features tend to coincide with the characteristic energies of slow phonons in a superconductor. These slow phonons are accumulated in the contact region, breaking effectively the Cooper pairs. This effect strongly enhances the intensity of the phonon spectral lines, which simultaneously modifies their shape. It is especially effective in the dirty contacts ($l_e << d$), where the intensity of the conventional phonon-induced backscattering processes are suppressed by the factor $\sim l_e/d$, and the slow phonon escape rate is further decreased by diffusion.

We will show below that in the $HoNi_2B_2C$ contacts a similar effect on the phonon-structure occurs due to the destruction of the magnetic order by nonequilibrium phonons. To distinguish this non-

equilibrium effect from the true thermal limit we shall call it the «quasi-thermal» limit. In this regime the nonequilibrium conduction electrons remain «cold», i.e., the Fermi distribution is smeared only by the environmental temperature [20] with an excess energy controlled by bias voltage.

In the present PCS study, we attempt to determine which interactions are the most efficient in the scattering of the conduction electrons in RNi_2B_2C. They are most likely the candidates to serve as mediators in the superconducting pairing mechanism. Although it was proposed that these materials fall into the class of common phonon-mediated superconductors [21], there is disagreement as to which phonons play a major role. Mattheiss, Siegrist, and Cava [22] emphasize the role of high energy ($\hbar\omega = 106$ meV) boron A_{1g} vibrations, while Pickett and Singh [23] estimate the characteristic Debye energy to be rather low (about 300 K) and point out the importance of low-energy phonon branches. The first point of view finds confirmation in the observation of an appreciable boron-isotope effect in YNi_2B_2C [24], while the second is consistent with the recent findings of phonon softening in $LuNi_2B_2C$ [25]. The controversy can be continued by mentioning the temperature dependence of the heat capacity of the nonmagnetic compound YNi_2B_2C driven to the normal state by magnetic fields, which shows an apparent lattice stiffening [26]. Moreover, the recent comparative study of the normal-state transport and magnetic properties of nonsuperconducting $LaNi_2B_2C$ and superconducting YNi_2B_2C and $HoNi_2B_2C$ (Ref. 27) have questioned the phonon-mediated superconducting pairing mechanism.

We have found reproducible peaks in the d^2V/dI^2 spectra of Ag(Cu)-RNi_2B_2C (R = Ho, Y) point-contacts situated at energies of about 4–20 meV. The positions of these features on the voltage axis correlate well with the characteristic energies of slow phonons found in the neutron measurements on $LuNi_2B_2C$ (Ref. 25) and YNi_2B_2C (Ref.28). The intensity of the soft phonon peaks in the PC EPI spectra of $HoNi_2B_2C$ can be suppressed by temperature and magnetic field, showing the anisotropy expected from the magnetic phase diagram [6]. In nominally nonmagnetic YNi_2B_2C the intensity of the soft phonon mode also depends on the magnetic field. The linear background in the PC spectra of both compounds corresponds to a quadratic energy dependence of the contact resistance and could originate from electron-electron or electron-magnon (paramagnon) scattering.

The high energy part of the PC spectrum of the Ho and Y compounds is dominated for most contacts by a background signal. The saturation of this background signal at about $eV \simeq 100$ meV coincides with the high-frequency boron-vibration energy and points to an appreciable EPI at this energy, as predicted by theory [22]. Nonetheless, comparing the PC spectra of Ho and YNi_2B_2C contacts, which reveal different superconducting properties, and taking into account the results of our PCS study of nonsuperconducting $LaNi_2B_2C$ (Ref. 29), we conclude that the low-energy part of the EPI spectra is mainly responsible for the Cooper pairing in these compounds.

2. Methodical details

The contacts are made by pressing together directly in the cryostat the sharp edge of a small silver (copper) bar to the *ab*-plane edge of $HoNi_2B_2C$ or YNi_2B_2C single crystals, which were prepared via the Ni_2B flux-growth method developed at Aims Laboratory [30]. During one run, many contacts with different contact resistances (in the range from several tenths to several tens of an Ohm) at different sites of the crystal surface could be created. Typical contact resistances chosen for the extensive temperature- and magnetic-field-dependent measurements are about 1 Ω, which corresponds to a contact size d of about 30 nm. This is of the same order of magnitude as the electron mean free path in the starting material at low temperatures. Thus, one may expect the spectroscopic regime of current flow not to be violated in the best contacts studied. Such contacts were chosen among many trials by looking at the Andreev reflection (AR) spectra $dV/dI(V)$ at $T << T_c$, which for the selected junctions reveal critical temperatures and superconducting energy gaps close to the following typical values: $T_c = 15.4$ K, $\Delta = 2.4 \pm 0.07$ meV and $T_c = 8.5$ K, $\Delta = 1.04 \pm 0.06$ meV for, respectively, the Y- and Ho-based compounds [31].

In Figs. 2,*a* and 2,*b* typical examples of the AR spectra for contacts with the Y and Ho compounds are shown, along with the fitting curves calculated according to the Blonder–Tinkham–Klapwijk–Dynes (BTKD) model [32]. The matching of the smearing parameter Γ (beyond the energy gap Δ_0 and barrier parameter Z) is essential in order to obtain a good fit for the two materials. The relatively large Γ values for the Ho compound are evidently connected with the magnetism in the superconducting state. Even for the nominally nonmagnetic Y-compound point contacts the BTKD-fit often does not follow the experimental points at

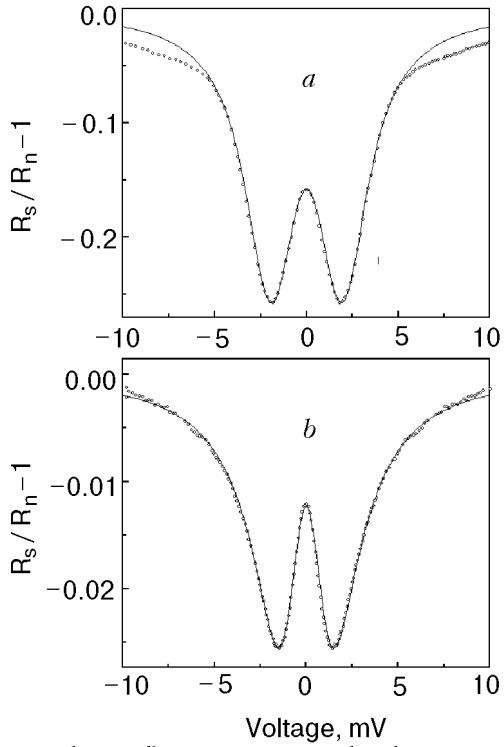

Fig. 2. Andreev reflection spectra in reduced units at $H = 0$ for YNi_2B_2C-Cu (a) and $HoNi_2B_2C$-Ag (b) point contacts. R_s and R_n are the $dV/dI(V)$ characteristics in the superconducting and normal states, respectively. The contact parameters and measurement conditions are: (a) $R_0 = 16.6\ \Omega$, $T_c = 15.4$ K, $T = 4.2$ K; (b) $R_0 = 0.77\ \Omega$, $T_c = 8.5$ K, $T = 1.6$ K. The solid curves represent the BTKD fits with the following parameters (see text): (a) $\Delta_0 = 2.1$ meV, $\Gamma = 0.6$ meV, $Z = 0.5$, $SF = 1.19$; (b) $\Delta_0 = 1.05$ meV, $\Gamma = 1.35$ meV, $Z = 0.595$, $SF = 0.58$.

energies greater than about 4 meV, as can be seen in Fig. 2,*a* and Fig. 12,*c*. As will be shown below, this energy corresponds to a maximum in the PC electron-phonon interaction spectral function for both YNi_2B_2C and $HoNi_2B_2C$. In $HoNi_2B_2C$ point-contacts similar kinks on the $R(V)$ curves are often more smeared due to the larger Γ values, as is the case in Fig. 2,*b*. It should be noted that actually the BTKD fitting procedure involves a fourth parameter, the scaling factor SF. This parameter scales the amplitude of the change in the dV/dI with a factor of order unity and may be due either to the nonhomogeneity of the boro-carbide compound in the contact region or to the asymmetry of the junction geometry.

Although for both compounds in Fig. 2 the barrier parameters Z do not differ much and the reduced temperatures T/T_c are both $<< 1$, the distance between dV/dI minima for the Ho compound ($2V_{min} = 1.48$ meV) differs noticeably from the energy gap $\Delta_0 = 1.05$ meV of the fitting curve due to extremely the large value of the Γ-parameter. Hence, one should be careful in identifying the energy gap parameter $2\Delta_0$ with $2V_{min}$ in the case of a large Γ.

The contact axis which determines the preferred direction of current flow is nominally parallel to the *ab*-plane. Its orientation with respect to the *a*(*b*)-crystallographic axis remains uncertain. A magnetic field up to 10 T can be applied either along the *ab*-plane or perpendicular to it. In the first case both parallel ($I \parallel H$) and perpendicular ($I \perp H$) orientations, with respect to the contact axis, have been investigated with not much difference in the results. Many different contacts were investigated and for the selected contacts a number of different characteristics were measured. Among them are temperature and magnetic field variations of $dV/dI(V)$, AR spectra, zero-bias magnetoresistance curves at different temperatures, point-contact spectra in the normal state [$d^2V/dI^2(V)$ characteristics] at various fields and temperatures.

In all the graphs we plot the second harmonic signal $V_{2F}(V)$, which is directly measured in experiments and which is connected with the $d^2V/dI^2(V)$ characteristics through the expression [15]

$$d^2V/dI^2(V) = 2\sqrt{2}R^2V_{2F}(V)/V^2_{mod}\ , \qquad (4)$$

where V_{mod} and $R = dV/dI$ are, respectively, the effective value of the modulation voltage and the differential contact resistance. The experimental data are scanned from $-V_{max}$ to $+V_{max}$ voltage bias to show the reproducibility of spectral features. The voltage polarity in all graphs corresponds to the polarity of the normal metal electrode (Cu, Ag). For plotting the EPI spectral function $g_{PC}(\omega)$ we use the odd part of the spectra $F_{odd}(V) = \frac{1}{2}[F(+V) - F(-V)]$, which contains the spectral information that does not depend on the voltage polarity and in most cases nearly coincides with the original curve. The modulation voltage V_{mod} and the temperature T determine the smearing of an infinitely narrow spectral peak according to the standard formula [16]

$$\delta V = \sqrt{(5.44k_BT/e)^2 + (1.72V_{mod})^2}\ . \qquad (5)$$

The results presented are representative of more than several hundred junctions that we have measured. While comparing our findings with the properties of bulk material one should keep in mind that the PC method probes a small volume with linear dimensions of the order of $d = 10$–100 nm, located at the crystal surface. Due to the extreme sensitivity of the material properties to small variations of the composition [13,33] some contacts show no superconductivity at all. Those contacts are dis-

carded. Those which remain after application of the selection criteria based on the AR spectra, still preserve some dispersion in composition and structural perfection of the material in the contact region, as well as in random deviations of the contact axis from the nominal orientation, which are probably the main cause of the variety of characteristics observed.

3. Experimental results

3.1. $HoNi_2B_2C$

Phonon structure for different regimes of current flow. In Fig. 3 we present the PC spectra for different $HoNi_2B_2C$-Ag contacts in the normal state at fields greater than $H_{c2}(0) \simeq 0.55$ T but less than 1–2 T at which, judging from the magnetization measurements [5,6,34], the magnetic order is not yet completely destroyed. There are some variations in the spectral line shapes which are due to the uncontrolled variations of the contact shape, the orientation of the probed crystallite, and the value of the elastic electron mean free path in the contact region, which leads to the different regimes of current flow. Judging from the width of the spectral lines compared with the expected smearing (Eq.(5)), one can tentatively assume the regime of current flow in contact 1 to be close to spectroscopic. On the other hand, the sharp «*N*»-type feature around ± 5 mV, with a negative overshooting with respect to the background in the PC spectrum of contact 3, resembles the quasi-thermal lineshape shown in Fig. 1,*d*. Similar negative overshooting is seen at about 20 meV in the spectrum of contact 2.

Despite these variations in lineshape, there are structures in the spectra of Fig. 3 at about 4–5 and 14–15 mV, which are common to all curves and which are marked by arrows. The lower energy is in striking correspondence with the characteristic energy of soft phonons, while the upper energy marks another characteristic phonon energy at which $\partial\omega/\partial q \simeq 0$ on the phonon dispersion curves of $LuNi_2B_2C$ [25]. In some spectra the wide low-energy peak at about 6 mV is further resolved into bands at 4 and 8 mV, which nicely fit in more detail the neutron data (see below). These observations support the recent neutron findings [25] and prove that soft phonons are involved in the spectral structure of the EPI in these compounds.

The fine structure of the low-energy part of the $HoNi_2B_2C$ EPI spectra is shown in Fig. 4 for two more contacts, which presumably corresponds to the spectroscopic conditions of the current flow. Be-

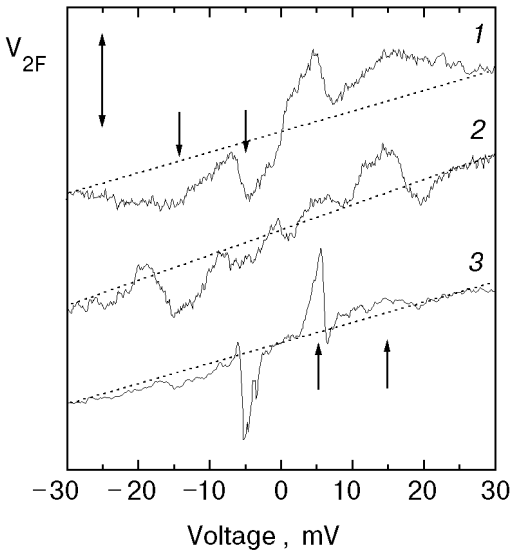

Fig. 3. Normal state point-contact spectra of $HoNi_2B_2C$-Ag contacts at $T = 1.6$ K. The contact resistance R, the magnetic field H, the modulation voltage V_{mod}, and the double-arrow bar for the calibration of the vertical axis are for each spectrum as follows: 0.7 Ω, 1.5 T, 0.7 mV, 0.21 μV (*1*); 0.53 Ω, 1 T, 0.9 mV, 0.55 μV (*2*); and 0.82 Ω, 0.7 T, 0.35 mV, 0.37 μV (*3*). Orientations of the contact axis (I) and magnetic field are for contacts 1 and 2 ($I \perp H$) $\perp c$, for contact 3 ($I \parallel H$) $\perp c$. The arrows mark the positions of the spectral bands common to all contacts. Dotted straight lines stand for the linear backgrounds. V_{2F} is the second harmonic signal which is proportional to the second derivative d^2V/dI^2 of the $I(V)$ characteristics [Eq. (4)]. For each curve $V_{2F} = 0$ at $V = 0$. Judging from the peak shapes the regimes of current flow can be classified as changing from spectroscopic (contact 1) to quasi-thermal (contact 3).

sides demonstrating that the spectral features do not depend on the contact resistance (size), these curves are evidence of the independence of the spectra on the material of the counter electrode. The positions of the maxima in the PC EPI spectra marked by arrows lie close to the characteristic $\partial\omega/\partial q \simeq 0$ phonon energies of the low-temperature phonon dispersion curves of $LuNi_2B_2C$ in the [ζ, 0, 0] direction [25], which are 4, 8.5, 14, and 19 meV at 10 K. If the dispersion curves for other directions would be known, a more detailed comparison with the total phonon density of states could be made. We emphasize that *all* PC EPI spectra of $HoNi_2B_2C$ contain the soft phonon maximum at about 4 meV.

Magnetic field dependence of phonon spectral peaks. Turning to the magnetic field dependence of the spectra, we first note that due to the preferential orientation of the Ho magnetic moments parallel to the *ab*-plane there is a strong anisotropy in magnetic properties of $HoNi_2B_2C$ [6,34,35]. Bearing this in mind, we first describe the influence

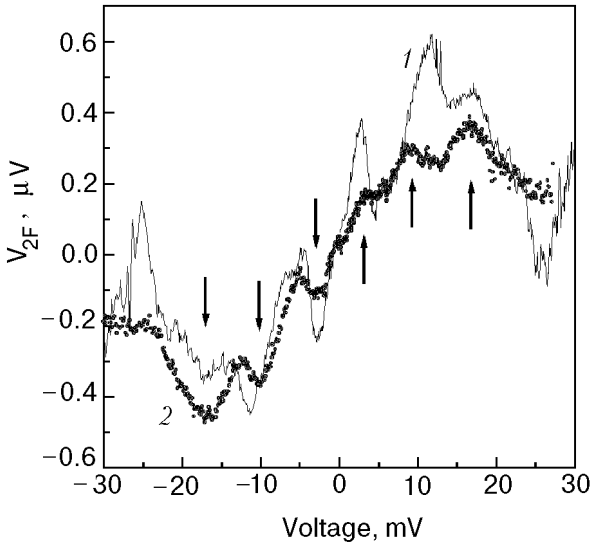

Fig. 4. Comparison of the phonon structure in the PC spectra of $HoNi_2B_2C$ with Ag (*1*) and Cu (*2*) counter electrodes at $T = 4.2$ K, $H = 1$ T. The parameters are: 1) $R = 0.85$ Ω, $V_{mod} = 0.6$ mV; 2) $R = 12$ Ω, $V_{mod} = 1$ mV. $I \parallel ab$, $H \parallel c$. The arrows mark the approximate peak positions common to both spectra.

of the magnetic field H parallel to the direction of easy magnetization, i.e., $H \parallel (ab)$.

A magnetic field $H \parallel (ab)$ strongly influences the spectral features at low energies. For typical junctions we have observed a suppression of the 4-meV peak by magnetic fields of the order of several tesla. This behavior is illustrated in Fig. 5, where the peak positions are marked by an arrow. We disregard the zero-bias peak in the differential resistance, which does not show a systematic behavior in magnetic field and has no relevance for the electron-phonon interaction. The magnetic-field range of the soft-phonon-peak depression extends up to 10 T. In Fig. 6 we show a contact with only a small influence of the field on the d^2V/dI^2-spectrum, where most of the phonon suppression occurs in fields up to about 2 T. Again, we regard the zero-bias anomaly as being nonessential for the phenomena considered here. Figure 7 shows a very strong magnetic field dependence for a contact with a spectrum similar to the one of contact 2 in Fig. 3, which clearly exhibits at 0.5 T the quasi-thermal-like «*N*»-type feature at 19 mV. It follows from Fig. 7 that fields up to about 2 T strongly suppress the intensity of phonon lines, modifying their shape and position on the voltage scale. On the other hand, fields greater than 2 T (and up to 9 T) do not change dramatically the PC spectrum in Fig. 7, which contains two maxima similar in shape, intensity, and energy position to those in Fig. 6.

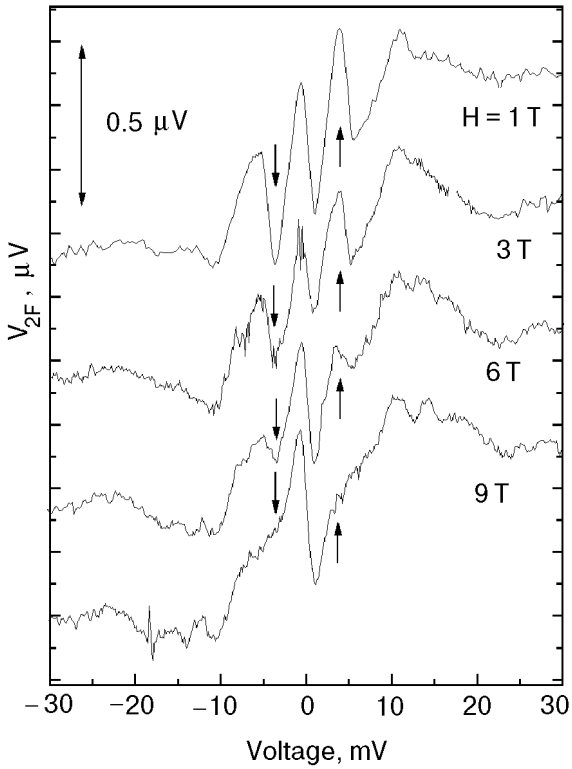

Fig. 5. The magnetic field dependence of the PC spectra for a $HoNi_2B_2C$-Ag contact, which shows the strong suppression of the 4-meV peak for the spectroscopic regime of the current flow. The curves are shifted vertically. For each curve $V_{2F} = 0$ at $V = 0$. $H \parallel (ab)$. $R = 2.66$ Ω, $V_{mod} = 0.7$ mV, and $T = 1.65$ K.

The contacts with $HoNi_2B_2C$ showed very often a suppression of the phonon structures by an applied magnetic field along the (ab)-plane. For this field orientation, the magnetic order is destroyed above about 1–2 T [5,6]. Therefore, we conclude that our data show a strong interaction between the magnon and phonon branches of the excitation spectra, which enhances the electron-phonon interaction with low-energy phonons in $HoNi_2B_2C$, and which is suppressed by magnetic fields that destroy magnetic order in this compound.

For $H \parallel c$ the magnetic structure of $HoNi_2B_2C$ is much more robust and does not experience strong changes in the range of magnetic fields studied. The upper superconducting critical magnetic field $H_{c2}(0)$ in $\parallel c$ direction is about the same as for $H \perp c$ [34]. Therefore, the superconductivity can be suppressed by $H \parallel c$ without influencing the magnetic order and without perturbing the phonon-magnon interaction. Two different junctions in Fig. 8 illustrate this behavior. The shape of the soft phonon feature at 3–5 mV remains almost unchanged in fields up to 7 T.

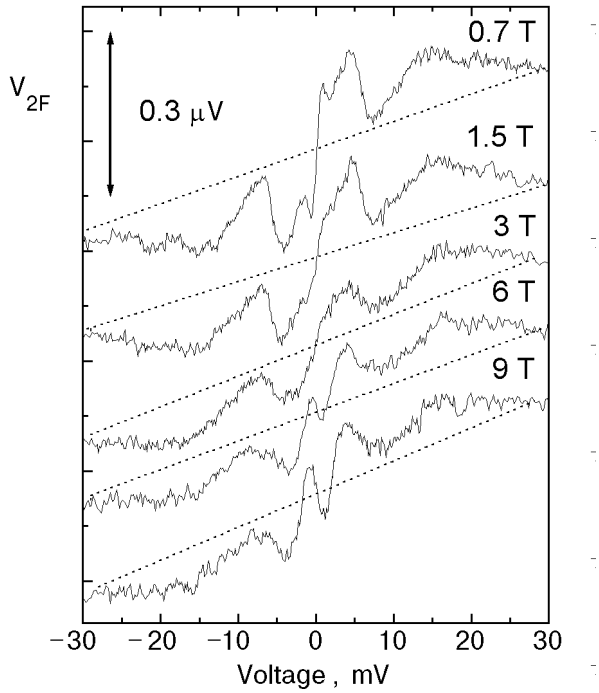

Fig. 6. The magnetic field dependence of the PC spectra for the $HoNi_2B_2C$-Ag point contact 1 in Fig. 3, which corresponds to the spectroscopic («nonthermal») regime of current flow. $R = 0.7$ Ω, $T = 1.6$ K, $V_{mod} = 0.7$ mV. The curves are shifted vertically for clarity. For each curve $V_{2F} = 0$ at $V = 0$ and the assumed linear background is shown by the dotted line. Mutual orientation of the contact axis, the magnetic field, and the crystallographic basal plane corresponds to $(I \perp H) \parallel ab$.

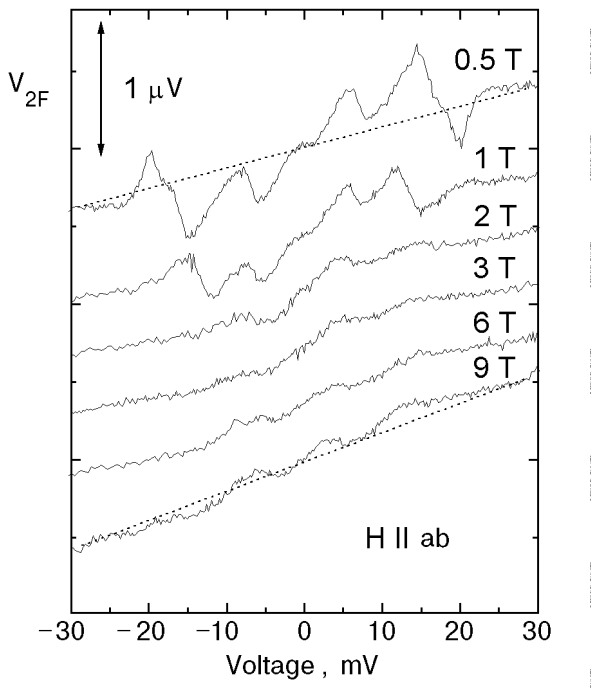

Fig. 7. The magnetic field dependence for a $HoNi_2B_2C$-Ag point contact, which shows the «quasi-thermal» negative overshooting beneath the linear background at fields of 0.5 and 1 T. $R = 0.5$ Ω, $V_{mod} = 0.8$ mV. The characteristics of this contact are very close to contact 2 in Fig. 3. The dotted straight lines represent the assumed backgrounds. For each curve $V_{2F} = 0$ at $V = 0$. Note the change of the phonon lineshape and the intensity for fields ≥ 2 T. $(I \perp H) \parallel ab$, $T = 4.2$ K.

Temperature dependence of PC EPI spectra. The most trivial effect of the temperature on the PC spectra is related to the thermal smearing of spectral features according to expression (5). For increasing temperatures, this effect should lead to an increase of the peak width and a decrease of its intensity in such a way that the area under the peak remains approximately constant. The position of the spectroscopic structure should remain fixed on the voltage axis.

The spectrum of a $HoNi_2B_2C$-Ag has been plotted in Fig. 9 for temperatures from 4.2 to 13 K. With rising temperature, the structure at about 5–6 mV moves to lower voltages, which is still close to the characteristic soft phonon energy of 3–4 meV. The inset in Fig. 9 shows the position V_1 of the low-energy maximum on the $V_{2F}(V)$ curves as a function of temperature. The intensity of this maximum disappears suddenly between 11 and 12 K. Such an abrupt disappearance of the spectral peak in a narrow temperature interval cannot be attributed to a simple temperature-induced broadening. This points to a transition at $T_m \sim 12$ K, which is either a first- or very steep second-order transition. At higher temperatures, only a very wide and shallow PCS maximum at about 15 meV is seen, which is not surprising since the spectral smearing [see Eq. (5)] is rather large at these temperatures. Note also the change in the shape and the increase in the intensity of the soft phonon spectral peak while passing from the curve taken at $T = 8$ K and $H = 1$ T to $T = 8.4$ K and $H = 0$, which corresponds to the partial restoration of the magnetic order. Such behavior definitely proves that magnetism is involved in the observation of the electron-phonon interaction at low energies.

The observed shift of the lowest energy-peak at about 3 meV to higher energies, while lowering the temperature, contradicts the softening of the phonon energy observed in neutron-scattering experiments for the case of $LuNi_2B_2C$ at low temperatures [25]. However, it corresponds to the temperature dependence of the 4-meV peak in neutron-scattering data on YNi_2B_2C [28].

Since the position of a true spectral peak should not depend on the temperature, we can conclude that the temperature dependence of the lowest energy peak in Fig. 9 corresponds to an intermediate

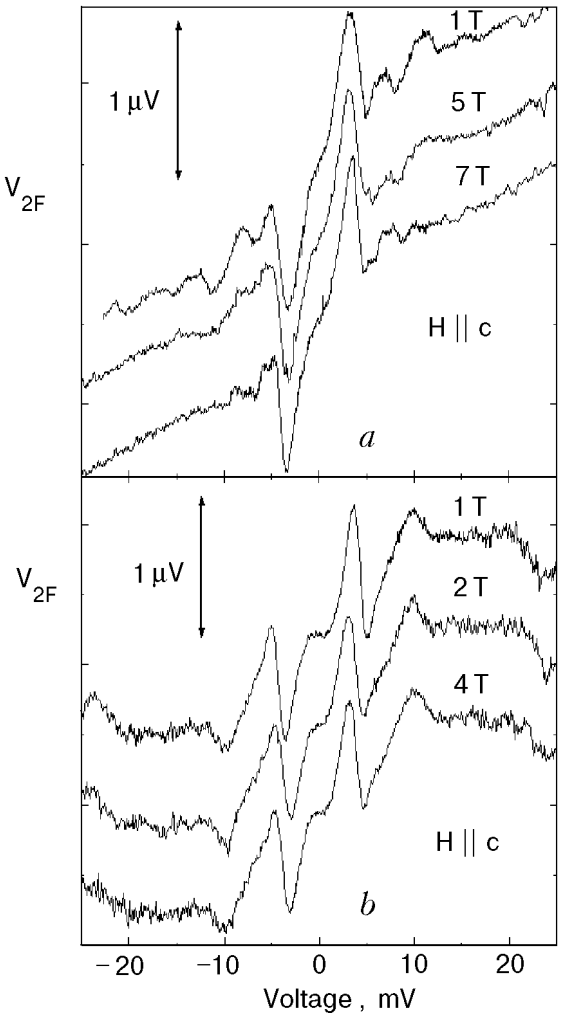

Fig. 8. The magnetic field dependences of the $HoNi_2B_2C$ PC spectra for $H \parallel c$ with Ag (*a*) and Cu (*b*) counter electrodes. The contact parameters and the measurement conditions are: (*a*) $R_0 = 1.51$ Ω, $V_{mod} = 0.5$ mV, $T = 4.2$ K; (*b*) $R_0 = 2.3$ Ω, $V_{mod} = 0.7$ mV, $T = 2.5$ K. Contact (*b*) is the same as in the lower panel of Fig. 13. For each curve $V_{2F} = 0$ at $V = 0$.

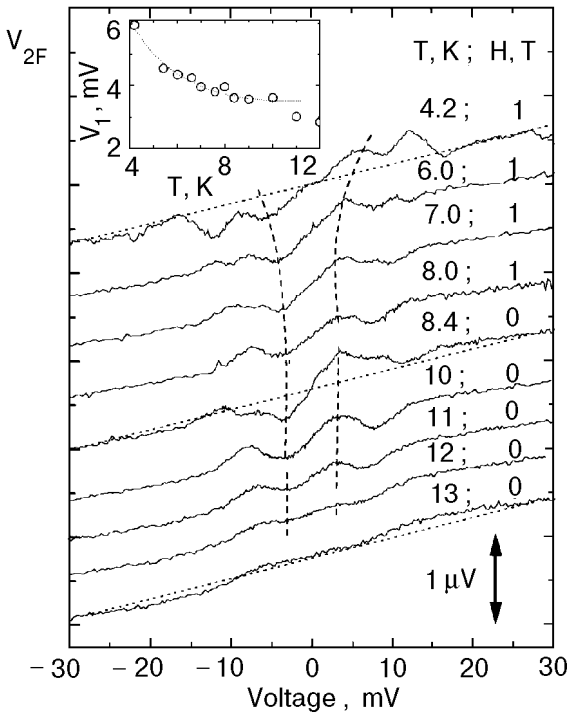

Fig. 9. The temperature dependence of the PC spectra for $HoNi_2B_2C$-Ag, which is similar to contact 2 in Fig. 3, and that shown in Fig. 7. $R = 0.62$ Ω, $V_{mod} = 0.95$ mV (for the uppermost curve $V_{mod} = 1.0$ mV). $(I \perp H) \parallel ab$. The temperatures and fields are indicated. The dotted straight lines mark the assumed backgrounds. The curves are shifted vertically for clarity. For each curve $V_{2F} = 0$ at $V = 0$. The dashed lines are intended to follow the temperature dependence of the low-energy peak position V_1 as a guide to the eye (see the inset).

regime of the current flow. At low temperatures the regime is quasi-thermal (where there is a noticeable dependence of the peak position V_1 on the bath temperature) and for higher temperatures it gradually transforms into a spectral regime (where the peak position is fixed) due to the suppression of the magnetic order at higher temperatures and the disappearance of the nonequilibrium effects. Such transformations of the regimes of current flow in the strongly coupled electron-phonon-magnon system are probably due to the peculiar temperature dependences of the nonequilibrium phonon and magnon escape and relaxation rates in a contact.

Unfortunately, we were not able to study the point contacts which satisfy the spectroscopic conditions in the whole temperature range and which are stable enough to survive the whole series of temperature-dependent measurements.

3.2. YNi_2B_2C

Phonon structure at low energies and its magnetic field dependence. The PC spectra for the nonmagnetic Y compound reveal a broad phonon peak at about 12 meV, which does not depend on the magnetic field (Figs.10,*a*, and 10,*b*). Because the same phonon structure is observed in Cu-YNi_2B_2C point contacts (Fig. 10,*b*), it is not due to a phonon contribution from the Ag electrode of the Ag-YNi_2B_2C contact. The absence of a Cu phonon band at 16–20 mV in the Cu-YNi_2B_2C contacts and the similarity of the PC spectra for the Cu-$HoNi_2B_2C$ and Ag-$HoNi_2B_2C$ contacts in Fig. 4 prove that the contribution of the noble metal electrodes to the spectra is strongly reduced, because the Fermi velocity in YNi_2B_2C and $HoNi_2B_2C$ is substantially smaller than in Cu(Ag), as predicted by band structure calculations [23].

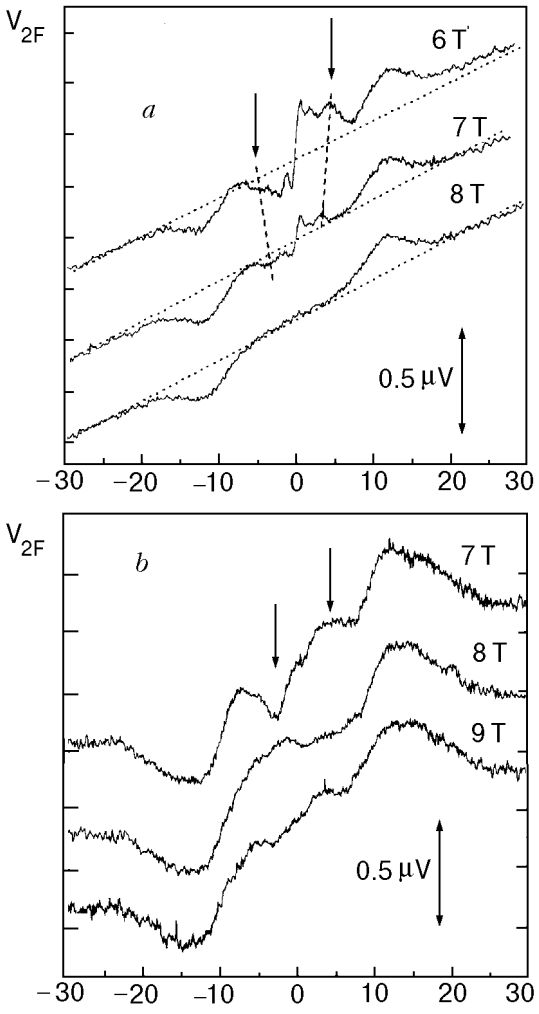

Fig. 10. The low energy parts of the PC spectra of YNi_2B_2C with Ag (a) and Cu (b) counter electrodes at different magnetic fields and $T = 4.2$ K, which show the magnetic field evolution of the 4-meV phonon structure. The parameters are: (a) $R = 1.8$ Ω, $V_{mod} = 0.6$ mV; (b) $R = 16.6$ Ω, $V_{mod} = 1.1$ mV. In panel (a) the structure at zero-bias at $H = 6$ and 7 T is due to the not fully suppressed superconducting state. The dashed lines through the spectral maxima serve as a guide to the eye. For each curve $V_{2F} = 0$ at $V = 0$. The dotted straight lines indicate the assumed backgrounds. The contact in panel (b) is the same as in the upper panel of Fig. 13.

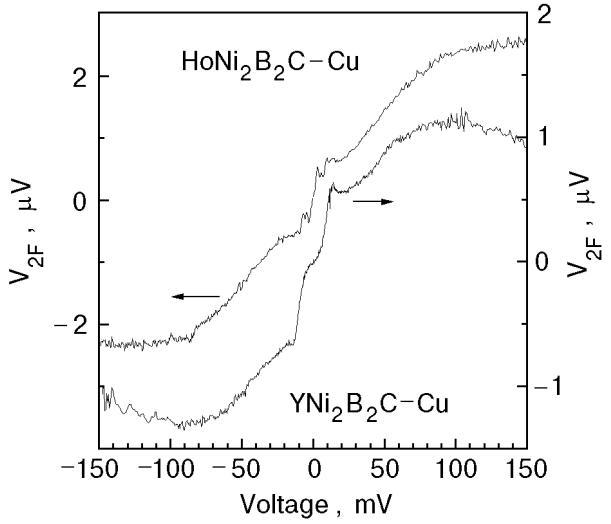

Fig. 11. The PC spectra where the boron vibrations at $eV \simeq 100$ mV take over at large biases, which presumably correspond to the thermal regime of the current flow. For the $HoNi_2B_2C$-Cu contact $R_0 = 1.91$ Ω, $V_{mod}(V = 0) = 0.55$ mV, and $H(\parallel c) = 0.6$ T; for the YNi_2B_2C-Cu contact $R_0 = 1.2$ Ω, $V_{mod}(V = 0) = 0.86$ mV, and $H(\perp c) = 6$ T. $T = 4.2$ K.

In the YNi_2B_2C contacts a weaker structure at about 4 meV, indicated by the arrows in Figs. 10,a and 10,b, is also observed. In order to study the normal state properties of these contacts, the applied magnetic field was above $H_{c2} = 5$–6 T in order to suppress the superconductivity in YNi_2B_2C. In the spectrum of Fig. 10,a a suppression of the low-energy phonon structure with a slight shift of the voltage position to lower values is observed in the limited field range from H_{c2} to 10 T. The spectrum in Fig. 10,b shows a nonmonotonic dependence on the magnetic field for the peak intensity, although without any change in the voltage position. A possible origin for the observed magnetic field dependence of this structure at low voltages could lay in the *magnetic interactions which would then even exist in the nominally nonmagnetic* YNi_2B_2C. Comparing the intensity of the 4-meV peak in YNi_2B_2C and $HoNi_2B_2C$ PC spectra, one should note that to destroy superconductivity in YNi_2B_2C one has to apply a much higher field than that in the case of $HoNi_2B_2C$. The applied fields, for YNi_2B_2C being in the normal state could already suppress the observed structure at 4 meV.

The spectra of the YNi_2B_2C contacts shown in Fig. 10 illustrate the difference in the regimes of current flow corresponding to the contacts of different resistances (sizes). The rapid suppression of the low-energy phonon peak (marked by the arrow) in Fig. 10,a and its shift to lower biases with increasing field resembles an analogous behavior of $HoNi_2B_2C$ contacts (see Fig. 7) in the quasi-thermal regime of the current flow. The smaller contact (Fig. 10,b) evidently is closer to the spectroscopic regime and, although the low-energy peak reveals a peculiar nonmonotonic dependence on the magnetic field, its position on the voltage scale remains fixed.

3.3. Evidence for high-frequency boron vibration mode

To cover the energy range including the A_{1g} boron vibration mode with a characteristic frequency corresponding to 106 meV (Ref. 23), we have to extend our point-contact measurements to voltages about an order of magnitude larger than in the data presented above. The increase of bias voltage leads to a gradual departure from the spectroscopic regime that approaches the thermal limit. Therefore, in the PC spectra of the $HoNi_2B_2C$-Cu and YNi_2B_2C-Cu contacts shown in Fig. 11, the initial parts with the low-frequency phonon spectral peaks gradually transform into a background signal, which is linear up to 50–70 meV and either saturates or has a shallow maximum at about = 100 meV. This energy marks the end of the phonon spectrum and coincides roughly with the high-frequency boron vibration mode. The observation of clear features at this energy points to an appreciable electron-phonon interaction with the A_{1g} boron mode.

4. Discussion

4.1. The origin of the spectral structure

Low-energy phonons as a primary source of spectral structure. The spectral structure at low bias voltages does not depend on the counter electrode (Cu, Ag). Its position on the voltage scale is independent of the magnetic field and temperature, provided their origin can be classified as «spectroscopic», i.e., satisfying the conditions of PCS [see Eq. (1)] without noticeable contact heating or nonequilibrium effects (see below).

We can prove in several ways that the maxima in the PC spectra at 4–5 and 10–15 meV correspond to the low-energy *phonons* in RNi_2B_2C. First, they are situated at the characteristic phonon energies found in $LuNi_2B_2C$ (Ref. 25) and YNi_2B_2C (Ref. 28) via neutron scattering experiments. Secondly, they are also observed at high fields, which completely destroy the magnetic order (Figs. 6 and 7) which excludes any magnetic origin of the observed structure (for instance, directly related to electron-magnon scattering).

Although we cannot measure the low-temperature PC spectra in the normal state unperturbed by the application of a magnetic field, there is evidence from the AR spectra at $H = 0$ that the 4-meV spectral structure is quite general for different RNi_2B_2C compounds, no matter which magnetic properties they possess. The typical examples for R = Ho, Er, and Y are demonstrated in Fig. 12. Although the shown AR spectra reveal quite different critical temperatures and superconducting energy gaps, they *deviate from the smooth BTKD behavior revealing a clear feature at* ~ 4 meV. The steep increase of the inelastic electron-scattering rate at this energy with a stepwise increase of the Γ-parameter could explain this feature. The characteristic energy is quite robust and does not depend on the contact resistance and the magnetic structure of the studied material, which proves its nonmagnetic origin.

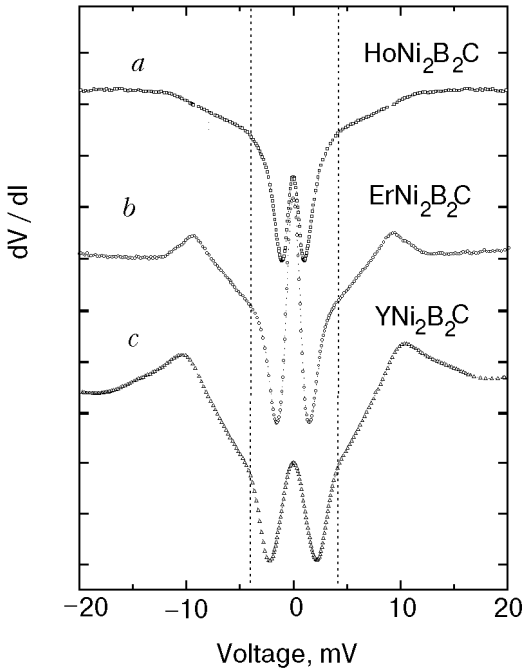

Fig. 12. The symmetrized Andreev reflection spectra [$dV/dI(V)$ dependences in the superconducting state] for the point contacts between Ag and RNi_2B_2C (R = Ho, Er, and Y). a) $HoNi_2B_2C$, R(20 mV) = 15 Ω, T = 1.6 K, 0.5 Ω per vertical division; b) $ErNi_2B_2C$, R(20 mV) = 0.33 Ω, T = 1.4 K, 0.023 Ω per division; c) YNi_2B_2C, R(20 mV) = 0.82 Ω, T = 4.2 K, 0.077 Ω per division. The vertical dotted lines mark the positions of the low-energy feature which is common to all spectra and which coincides with the lowest characteristic phonon energy in $LuNi_2B_2C$ (Ref. 25). $T << T_c$.

It is interesting to note that in metallic Ho there is also a strong optical magnon band at $\hbar\omega$ = 4 meV (Ref. 37). This suggests that in magnetically ordered $HoNi_2B_2C$ the crossing of low-energy phonon and magnon branches might lead to the appearance of a low-energy mixed phonon-magnon excitation-branch due to the repulsion of energy bands. Further investigations with polarized neutron scattering should clarify this point.

Quasi-thermal enhancement of phonon spectral line intensity. In many cases the observed peaks are not the conventional bell-shaped phonon peaks, but rather N-type shaped structures. After subtracting

the linear background, the N-type shape corresponds more to maxima on the dV/dI curves than on the $d^2V/dI^2(V)$ dependences. These observations support our view that the N-shaped peaks, though located *close* to the characteristic phonon energies, are not simply due to the inelastic backscattering of conduction electrons by phonons, as is the case for the standard PCS [15,16]. The following observations relate these N-shaped phonon peaks to the destruction of magnetic order.

The positions and intensities of the N-shaped structures decrease with increasing magnetic field. At low fields the shape changes drastically and the intensity is strongly suppressed. At fields above the paramagnetic saturation field of about 1–2 T [5,6], the structure becomes only weakly magnetic-field dependent and looks as traditional, smeared PCS maxima. This described behavior is characteristic of the point-contact experiments with the magnetic $HoNi_2B_2C$. It originates from the strong coupling between the vibrational and magnetic degrees of freedom in this compounds. The strong phonon-magnon coupling easily leads to a large deviation from equilibrium in the phonon-magnon system, which is driven by the electrons that pass through the contact. The deviation from equilibrium is especially important in large and dirty contacts, since the escape rate of the nonequilibrium quasi-particles is hindered there by diffusion in the contact region. In small, clean contacts the nonequilibrium quasi-thermal effects are negligible due to the fast ballistic escape of the nonequilibrium quasi-particles from the contact region.

We propose the following explanation of the nonequilibrium phenomena observed in $HoNi_2B_2C$ point contacts which is, so to speak, a «magnetic» version of the earlier-found strong enhancement of the phonon structure by nonequilibrium phenomena in superconducting point contacts [19]. The ballistically injected nonequilibrium electrons generate *slow phonons* each time the bias voltage approaches an energy corresponding to the flattening of the phonon dispersion curves. At these biases the phonon branches have maxima in the density of state and their group velocities tend to zero. Those phonons cannot escape from the contact and thermalize through phonon-phonon collisions. Due to the *coupling between the phonon and magnon excitations*, which we assume to be strong, the magnon subsystem equilibrates with the phonons and the magnetic order is destroyed upon reaching the critical temperature of magnetic ordering in a given magnetic field. In fact, the thermalization of the phonon-magnon system is not necessary provided that the concentration of nonequilibrium magnetic excitations becomes large enough to destroy the magnetic order. Since the critical conditions depend on the complicated balance between the generation, escape, and decay rates of various quasi-particles (electrons, phonons, and magnons), where the phonons are only one of the few constituents in this picture, the position of a «N»-type feature on the voltage scale is only approximately fixed around the characteristic phonon energies which become temperature- and magnetic-field dependent. At the corresponding critical bias voltages for the destruction of the magnetic order, the resistance of a point contact reveals a sharp increase. The resulting N-shaped structure in the PC spectra is similar to that found in the point contacts with the ferromagnetic metals of the iron group, where the magnetic transition is driven by Joule heating of the contact region at much larger biases [17]. Quantitatively, for a slow boson subsystem it is possible to be heated up to a temperature $\leq T_0 \sim (eV/4k_B)$ without temperature smearing of the electron distribution [20]. The steep rise of the contact resistance that occurs at about 5 mV then corresponds to T_0, which is roughly equal to the temperature at which the magnetic order is destroyed. Such an estimate gives the magnetic ordering temperature T_{mag} with an upper bound of 14.5 K, which roughly corresponds to our observations of $T_{mag} = 11–12$ K (see Fig. 9) and to the neutron powder-diffraction results of $T_{mag} \sim 8–10$ K. Since the point contacts are located close to the crystal surface, we compare our results with the neutron measurements on powders [5,38], rather than with the bulk single-crystal results with $T_{mag} \sim 6$ K. [7]

Magnetic field dependence of the soft phonon branch. The low-energy phonon peak in the Ho compound appears to be very sensitive to the magnetic field parallel to the *ab*-plane, which points to the strong interaction between phonons and magnons. Our findings support the suggestion [25] that the phonon softening down to 4 meV is connected with the appearance of the incommensurate spin-density-wave along the *a(b)* crystal axis in Er and Ho compound, since both occur at about the same wave vectors (close to $a^* = 0.55$ [7,39]), which correspond to the nesting of the Fermi surface [40]. We have shown that the 4-meV spectral feature is also present in $ErNi_2B_2C$ (see Fig. 12). It is possible that the spin-density wave is present also in the Y compound, where a magnetic field could destroy the nesting feature that gives rise to the phonon softening.

In the above-described scenario, the lattice softening and the establishment of the magnetic order in the *a(b)*-direction cooperate with each other in lowering the total energy of a metal. If the soft phonon modes are important in the Cooper pairing, then the much stronger influence of magnetic field on the mixed electron-magnon-phonon interaction for $H \parallel ab$ should contribute to the anisotropy (or, more correctly, the apparent isotropy [34]) of H_{c2} in this material.

The dependence of the low-energy PCS phonon structure on magnetic field found in our experiments implies that the soft phonon modes *measured by neutrons* at low temperatures in $HoNi_2B_2C$ should reveal a strong sensitivity to the external magnetic field. It would be very interesting to check this prediction.

4.2. The linear background and interaction of electrons with non-phononic excitations

Many point-contact spectra on YNi_2B_2C, as well as on $HoNi_2B_2C$ (see, for example, Figs. 6, 7, and 10,*a*), reveal a linear background signal starting from low bias voltages. Such a behavior is atypical for point contact spectra of conventional metals and alloys. If the electron-phonon interaction dominates, the background is due to the additional scattering of the conduction electrons on the generated nonequilibrium phonons in the contact area and results in a signal which corresponds to an energy integral of the phonon density of states. One of the reasons of the observed anomalous linear background signal could be that electron-electron (or electron-paramagnon [36]) interactions with a quadratic energy dependence in the scattering rate are strong scatters of the conduction electrons in these systems.

It follows from our measurements that the electron scattering by non-phononic excitations in YNi_2B_2C and $HoNi_2B_2C$ is essential up to energies of the order of 50 meV (Fig. 11), which correspond to the biases at which the contact resistance has an inflection point. This feature is clearly seen as a broad maximum at about 50 meV in the second harmonic signal for a number of contacts (not shown) along with another typical behavior of the background characterized by a saturation or wide shallow maximum at the boron vibration energy ~ 100 meV, shown in Fig. 11. In the thermal regime of the current flow the maximum temperature in the contact is $T_0 \simeq V/2\sqrt{L}$ [Eq. (3)]. This would correspond to a $\rho_{bulk}(T)$ dependence which has an inflection point at about 160 K, nicely fitting what is observed in the experiment [27].

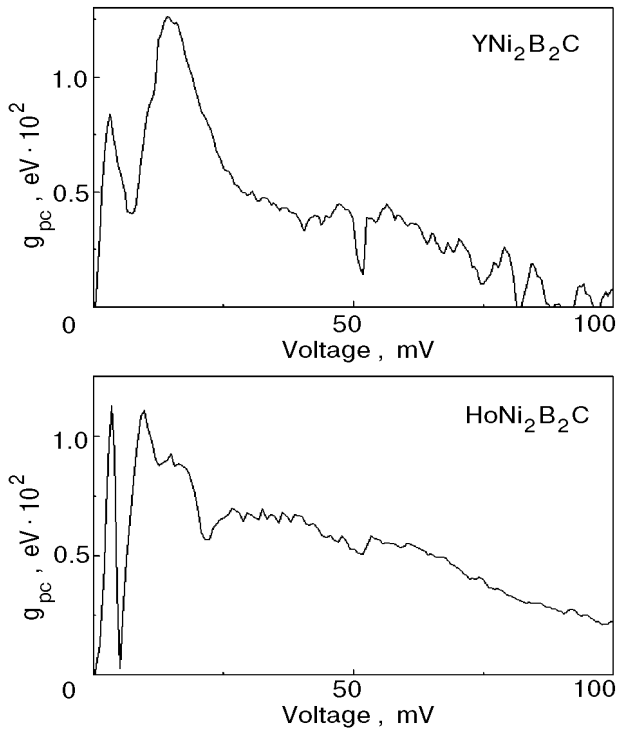

Fig. 13. The PC EPI spectral functions $g_{PC}(\omega)$ [see Eq. (2)] of YNi_2B_2C (upper panel) and $HoNi_2B_2C$ (lower panel) obtained as described in Ref. 29. The calculated λ_{PC} parameters are 0.05 and 0.1 for, respectively, YNi_2B_2C and $HoNi_2B_2C$.

4.3. The boron vibrations, electron-phonon spectral functions, and λ parameters

After subtracting a smooth background from the measured d^2V/dI^2 spectra in the spectroscopic regime, the EPI spectral function $g_{PC}(\omega) = \alpha^2_{PC}(\omega)F(\omega)$ can be obtained using Eq. (2) for the scaling. The obtained EPI spectral functions for YNi_2B_2C and $HoNi_2B_2C$ are shown in Fig. 13 (Ref. 29). By analogy with the conventional EPI parameter $\lambda = 2\int \alpha^2F(\omega)d\omega/\omega$, the $\lambda_{PC} = 2\int \alpha^2_{PC}F(\omega)d\omega/\omega$ parameter can be calculated from the spectra [16]. The obtained values for λ_{PC} are of the order of 0.01 for typical spectra, which reach 0.1 for the most intensive spectrum, which is at least an order of magnitude smaller than expected from the band structure calculations [23]. This discrepancy may be partly due to the short electron mean free path l_e for elastic scattering, which leads to the diffusive regime of the current flow, $l_e << d << \sqrt{l_e l_{in}}$, in the contact region. In this case the contact diameter d in Eq. (2) should be replaced by l_e . The electron mean free path in the bulk is 10–100 nm (from $pl \sim 10^{-11}$ Ω·cm^2, as for a standard free electron metal, and the resistivity $\rho \sim 10^{-6}$–10^{-5} Ω·cm[4]) is of the same order of magnitude as the contact diameter calculated from

the contact resistance, $R_0 \sim 1\ \Omega$, in the diffusive limit $d \sim \rho/R_0$. The maximum realistic shortening of l_e by static imperfections down to 1 nm can account for roughly an order-of-magnitude suppression of the spectral intensity [18]. The additional suppression may be due to unknown effects, which are related to the barrier at the contact interface or to a possibly small fraction of the contact that contributes to the phonon structure.

The boron vibrational spectral band at about the expected 100 meV is seen in many of the PC spectra as a broad maximum or as a change in the $d^2V/dI^2(V)$ slope that tends to saturation at voltages approximately equal to 100 mV (see Fig. 11). The dominating role of the boron vibrations in the overall background behavior in many of the PC spectra clearly points to a contribution of the boron vibrational modes to the interaction parameter λ. However, we observed also spectra in which the prominent structure at 100 meV is absent, although a clear AR energy-gap structure suggests that the material under the contact is superconducting [29]. This may be due either to the strong anisotropy of the EPI (i.e., that for certain orientations of the contact axis the boron vibrations are not seen in the PC spectra) or to the fact that the high energy boron vibrations are not of great significance for the superconducting state. For some contacts with the YNi_2B_2C and $HoNi_2B_2C$ single crystals, with the contact axis oriented parallel to the c direction, we observed spectra (not shown here) with a strong boron feature at about 100 meV, but with neither low-frequency phonon peaks nor superconductivity under the contact. On the other hand, there are spectra of $HoNi_2B_2C$, in which any structure at about 100 meV is absent but the superconductivity under the contact is present, as revealed by the AR dependences (together with the intensive low-frequency phonon peaks). These observations suggest that the EPI with the high-frequency boron mode, although being quite appreciable, is not vitally important for the superconductivity in these materials.

The quantitative estimates and even the relative comparison of the intensities of low-energy and high-energy phonon peaks cannot be made since the regime changes from the spectroscopic to the thermal one, while increasing the bias from the mV range to 100 mV. The developing fluctuations at $eV \geq 100$ meV also point to a strong heating inside the contact region (Fig. 11).

Conclusions

We have shown the possibility of the application of point-contact spectroscopy to study the electron-quasiparticle-interaction spectral function in superconducting and magnetic rare-earth nickel boro-carbides. To the best of our knowledge, until now this is the only experimental technique able to yield information on the given issue. The dominating scattering mechanism for conduction electrons appears to be the electron-phonon interaction. The strong interaction with a soft phonon mode ($\hbar\omega \simeq 4$ meV) is clearly observed in the PC spectra. At low energies ($eV < 20$ meV) there is an enhancement of the electron-phonon interaction by magnetic order in $HoNi_2B_2C$, which may support the superconducting state in this material. The intensity of these phonon peaks is suppressed by the magnetic field in $HoNi_2B_2C$ in an anisotropic way, pointing to an interaction between the phonons and the magnetic system. Unexpectedly, in nominally nonmagnetic YNi_2B_2C a magnetic field was found to influence the intensity of the low-energy spectral peak, pointing to the existence of magnetic interactions in this compound. Comparing our results with the bulk resistivity measurements of Fisher et al. [27], we suggest that the electron-magnon(paramagnon) interaction in $HoNi_2B_2C$ and YNi_2B_2C might be what distinguishes their $\rho_{bulk}(T)$ dependences from that for the nonsuperconducting $LaNi_2B_2C$.

The comparison of the EPI spectra of superconducting YNi_2B_2C and $HoNi_2B_2C$ with the nonsuperconducting $LaNi_2B_2C$ [29], as well as the comparative study of PC-EPI and AR spectra for various contacts with superconducting Ho- and Y-based compounds undertaken in this work, suggest that the low-energy part of electron-quasiparticle-interaction spectral function is responsible for the Cooper pairing in these materials. The strong electron-phonon-(para)magnon coupling observed in the case of magnetic $HoNi_2B_2C$ and nominally nonmagnetic YNi_2B_2C makes it problematic that these materials belong to the family of the ordinary electron-phonon-coupled superconductors, but rather attaches them to the high-T_c and heavy fermion systems.

I. K. Y. and V. V. F. acknowledge the financial support by the European Community grant INTAS-94-3562 and the Soros Foundation. Ames Laboratory is operated for the U. S. Department of Energy by Iowa State University under Contract No. W-7405-Eng-82. The work in this Laboratory was supported by the Director for Energy Research, Office of Basic Energy Sciences.

1. R. Nagarajan, C. Mazumdar, Z. Hossain, S. K. Dhar, K. V. Gopalakrishnan, L. C. Gupta, C. Godart, B. D. Padalia, and R. Vijayaraghavan, *Phys. Rev. Lett.* **72**, 274 (1994).

2. R. J. Cava, H. Takagi, H. W. Zandbergen, J. J. Krajewski, W. F. Peck, Jr., T. Siegrist, B. Batlogg, R. B. van Dover, R. J. Felder, K. Mizuhashi, J. O. Lee, H. Eisaki, and S. Uchida, *Nature* **367**, 146 (1994).
3. O. Fisher, *Magnetic Superconductors in Ferromagnetic Materials*, E. P. Wohlfarth (ed.), North-Holland, Amsterdam (1990), vol. 5.
4. H. Eisaki H. Takagi, R. J. Cava, B. Batlogg, J. J. Krajewski, W. F. Peck, Jr., K. Mizuhashi, J. O. Lee, and S. Uchida, *Phys. Rev.* **B50**, 647 (1994).
5. T. E. Grigereit, J. W. Lynn, Q. Huang, A. Santoro, R. J. Cava, J. J. Krajewski, and W. F. Peck, Jr., *Phys. Rev. Lett.* **73**, 2756 (1994).
6. P. C. Canfield, B. K. Cho, D. C. Johnston, D. K. Finnemore, and M. F. Hundley, *Physica* **C230**, 397 (1994).
7. A. I. Goldman, C. Stassis, P. C. Canfield, J. Zarestky, P. Dervenagas, B. K. Cho, D. C. Johnston, and B. Sternlieb, *Phys. Rev.* **B50**, 9668 (1994).
8. M. E. Hanson, F. Lefloch, W. H. Wong, W. G. Clark, M. D. Lan, C. C. Hoellwarth, R. Klavins, and R. N. Shelton, *Phys. Rev.* **B51**, 674 (1995).
9. T. Jacobs, B. A. Willemsen, S. Sridhar, R. Nagarajan, L. C. Gupta, Z. Hossain, C. Mazumdar, P. C. Canfield, and B. K. Cho, *Phys. Rev.* **B52**, R7022 (1995).
10. L. P. Le, R. H. Heffner, J. D. Thompson, D. E. MacLaughlin, G. J. Nieuwenhuys, A. Amato, R. Feyerherm, F. N. Gygax, A. Schenck, P. C. Canfield, and B. K. Cho, *Phys. Rev.* **B53**, R510 (1996).
11. T. Ekino, H. Fujii, M. Kosugi, Y. Zenitani, and J. Akimitsu, *Physica* **C235–240**, 2529 (1994).
12. T. Hasegawa, M. Ogino, A. Takagi, E. Watanabe, M. Nantoh, H. Takagi, S. Uchida, R. J. Cava, and K. Kitazawa, *Physica* **C235–240**, 1859 (1994).
13. E. Bar-Sadeh, I. Felner, U. Asaf, and O. Millo, *Phys. Rev.* **B52**, 6734 (1995).
14. G. T. Jeong, J. I. Kye, S. H. Chun, Z. G. Khim, W. C. Lee, P .C. Canfield, B. K. Cho, and D. C. Johnston, *Physica* **C253**, 48 (1995).
15. A. G. M. Jansen, A. P. van Gelder, and P. Wyder, *J. Phys.* **C13**, 6073 (1980).
16. A. V. Khotkevich and I. K. Yanson, *Atlas of Point Contact Spectra of Electron-Phonon Interactions in Metals*, Kluwer Academic, New York (1995).
17. B. I. Verkin, I. K. Yanson, I. O. Kulik, O. I. Shklyarevskii, A. A. Lysykh, and Yu. G. Naidyuk, *Solid State Commun.* **30**, 215 (1979).
18. I. K. Yanson and O. I. Shklyarevskii, *Sov. J. Low Temp. Phys.* **12**, 509 (1986).
19. I. K. Yanson, V. V. Fisun, N. L. Bobrov, and L. F.Rybal'chenko, *JETP Lett.* **45**, 543 (1987).
20. I. O. Kulik, A. N. Omel'yanchuk, and I. K. Yanson, *Fiz. Nizk. Temp.* **7**, 263 (1981) [*Sov. J. Low Temp. Phys.* **7**, 129 (1981)].
21. S. A. Carter, B. Batlogg, R. J. Cava, J. J. Krajewski, and W. F. Peck, Jr., *Phys. Rev.* **B50**, 4216 (1994).
22. L. F. Mattheiss, T. Siegrist, and R. J. Cava, *Solid State Commun.* **91**, 587 (1994).
23. W. E. Pickett and D. J. Singh, *Phys. Rev. Lett.* **72**, 3702 (1994).
24. D. D. Lawrie and J. P. Frank, *Physica* **C245**, 159 (1995).
25. P. Dervenagas, M. Bullock, J. Zarestky, P. Canfield, B. K. Cho, B. Harmon, A. I. Goldman, and C. Stassis, *Phys. Rev.* **B52**, R9839 (1995).
26. N. M. Hong, H. Michor, M. Vybornov, T. Holubar, P. Hundegger, W. Perthold, G. Hilscher, and P. Rogl, *Physica* **C227**, 85 (1994).
27. I. R. Fisher, J. R. Cooper, and R. J. Cava, *Phys. Rev.* **B52**, 15086 (1995).
28. H. Kawano, H. Yoshizawa, H. Takeya, and K. Kadowaki, *Czech. J. Phys.* **46**, S2–825 (1996); *Phys. Rev. Lett.* **77**, 4628 (1996).
29. I. K. Yanson, V. V. Fisun, A. G. M. Jansen, P. Wyder, P. C. Canfield, B. K. Cho, C. V. Tomy, and D. McK. Paul, *Phys. Rev. Lett.* **78**, 935 (1997).
30. M. Xu, P. C. Canfield, J. E. Ostenson, D. K. Finnemore, B. K. Cho, Z. R. Wang, and D. C. Johnston, *Physica* **C227**, 321 (1994).
31. L. F. Rybaltchenko, I. K. Yanson, A. G. M. Jansen, P. Mandal, P. Wyder, C. V. Tomy, and D. McK. Paul, *Physica* **B218**, 189 (1996).
32. A. Plecenik, M. Grajcar, S. Benacka, P. Seidel, and A. Pfuch, *Phys. Rev.* **B49**, 10016 (1994).
33. H. Schmidt, M. Weber, and H. F. Braun, *Physica* **C246**, 177 (1995); *ibid* **256**, 393 (1996).
34. K. D. D. Rathnayaka, D. G. Naugle, B. K. Cho, and P. C. Canfield, *Phys. Rev.* **B53**, 5688 (1996).
35. B. K. Cho, B. N. Harmon, D. C. Johnston, and P. C. Canfield, *Phys. Rev.* **B53**, 2217 (1996).
36. D. L. Mills, *J. Phys. Chem. Solids* **34**, 679 (1973).
37. M. W. Stringfellow, T. M. Holden, B. M. Powell, and A. D. B. Woods, *J. Phys. C: Metal Phys. Suppl.* No. 2, **3**, S189 (1970).
38. J. W. Lynn, Q. Huang, A. Santoro, R. J. Cava, J. J. Krajewski, and W. F. Peck, Jr., *Phys. Rev.* **B53**, 802 (1996).
39. J. Zarestky, C. Stassis, A. I. Goldman, P. C. Canfield, P. Dervenagas, B. K. Cho, and D. C. Johnston, *Phys. Rev.* **B51**, R678 (1995).
40. J. Y. Rhee, X. Wang, and B. N. Harmon, *Phys. Rev.* **B51**, 15585 (1995).